Article

Not peer-reviewed version

Gas-Phase Phosphate Surface Modification of Iron Powders: Microstructural Evolution and Coating Formation Mechanisms

Mirzokhid A. Tukhtabayev * , Abdukayum R. Normirzaev , Olga F. Minchukova , Aliaksandr L. Zhaludkevich

Posted Date: 5 March 2026

doi: 10.20944/preprints202603.0460.v1

Keywords: gas-phase phosphating; iron powders; surface modification; phosphate coating; microstructural evolution; powder metallurgy; surface engineering; phase stability doi:10.20944/preprints202603.0460.v1

Article

Gas-Phase Phosphate Surface Modification of Iron Powders: Microstructural Evolution and Coating Formation Mechanisms

Mirzokhid A. Tukhtabayev [1,*], Abdukayum R. Normirzaev [2], Olga F. Minchukova [2] and Aliaksandr L. Zhaludkevich [2]

[1] Namangan State Technical University, Namangan, 160103, Uzbekistan
[2] Scientific Practical Materials Research Centre of NAS of Belarus, Minsk, 220072, Belarus
* Correspondence: mirzoxidta@gmail.com; Tel.: +998977600462

Abstract

Surface modification of metallic powders plays a critical role in improving their chemical stability, interfacial characteristics, and processing behavior in powder metallurgy applications. In this study, micron-sized iron powders were treated using a controlled gas-phase phosphating process to investigate surface layer formation and microstructural evolution. The influence of treatment conditions on phase stability, surface morphology, and elemental distribution was systematically analyzed using X-ray diffraction (XRD), scanning electron microscopy (SEM), and energy-dispersive spectroscopy (EDS). The results confirm the preservation of the body-centered cubic α-Fe phase within an optimized temperature range, while a conformal phosphate-based surface layer was successfully formed. Increased treatment severity led to partial surface oxidation and localized microstructural heterogeneity. Elemental mapping revealed homogeneous phosphorus distribution under controlled processing conditions, indicating uniform coating development. The study establishes clear correlations between gas-phase processing parameters and surface layer formation mechanisms. These findings provide insight into the controlled surface engineering of iron powders and offer practical guidance for optimizing gas-phase phosphating routes in advanced powder metallurgy and metallurgical applications.

Keywords: gas-phase phosphating; iron powders; surface modification; phosphate coating; microstructural evolution; powder metallurgy; surface engineering; phase stability

---

1. Introduction

Surface engineering of metallic powders has become an essential approach for tailoring their chemical stability, interfacial behavior, and processing performance in advanced metallurgical applications [1–3]. In powder metallurgy and related manufacturing technologies, the surface condition of metallic particles plays a decisive role in oxidation resistance [4,5], interparticle bonding, compaction behavior, and overall structural integrity. Among metallic systems, iron powders are widely used due to their cost-effectiveness, mechanical strength, and broad applicability in structural components and functional materials. However, their high surface reactivity and susceptibility to oxidation necessitate controlled surface modification strategies.

Phosphating is a well-established surface treatment technique traditionally applied to bulk steel components to improve corrosion resistance and coating adhesion [2,6]. In powder systems, phosphate-based surface layers can serve as protective barriers, modify interfacial chemistry [7–9], and influence subsequent processing steps. Conventional phosphating methods are predominantly liquid-phase processes [10,11], involving aqueous solutions that promote chemical conversion reactions at the metal surface. While effective, wet phosphating of powders often presents challenges such as uneven layer formation, residual contamination, particle agglomeration, and limited control over coating uniformity at the microscale.

Gas-phase surface modification has emerged as a promising alternative that enables improved process control and homogeneous treatment of individual particles [12,13]. In gas-phase phosphating, reactive species are delivered under controlled thermal and atmospheric conditions, allowing conformal surface layer formation without direct liquid-solid interactions. This approach minimizes agglomeration and facilitates uniform exposure of micron-sized particles. Despite these advantages, systematic studies addressing the influence of gas-phase treatment parameters on phase stability and surface layer development in iron powders remain limited [14–16].

A critical aspect of gas-phase surface engineering is the balance between coating formation and preservation of the metallic core. Iron is prone to oxidation at elevated temperatures, and excessive treatment severity may induce undesirable phase transformations or surface oxide formation. Such transformations can alter crystallographic structure, modify surface morphology, and compromise coating uniformity. Therefore, identifying optimized processing windows that enable phosphate layer formation while maintaining structural stability is essential for reliable application [17,18].

Previous investigations have often focused on reporting successful coating formation or qualitative surface observations, with limited emphasis on establishing quantitative correlations between processing parameters and microstructural outcomes. However, for practical implementation in powder metallurgy, understanding process-structure relationships are crucial. Treatment temperature and exposure time influence diffusion kinetics, reaction rates, nucleation of phosphate species, and interfacial stability. A systematic evaluation of these parameters provides insight into coating development mechanisms and enables optimization of surface engineering strategies.

Microstructural characterization techniques play a key role in assessing the effectiveness of surface modification. X-ray diffraction (XRD) enables evaluation of phase stability and detection of possible oxidation products. Scanning electron microscopy (SEM) provides direct observation of morphological changes and coating continuity, while energy-dispersive spectroscopy (EDS) allows analysis of elemental distribution and confirmation of phosphate incorporation. The integration of these techniques offers a comprehensive understanding of surface layer evolution under varying treatment conditions.

The present study aims to establish clear correlations between gas-phase phosphating parameters and the structural evolution of micron-sized iron powders. Particular attention is given to phase stability, surface morphology, and elemental homogeneity under different processing conditions. By systematically analyzing treatment temperature and exposure effects, this work identifies optimized processing windows for stable and uniform surface layer formation. The findings contribute to the controlled surface engineering of iron powders and provide practical guidance for their application in powder metallurgy and advanced metallurgical systems.

2. Materials and Methods

2.1. Starting Materials

Commercially available water-atomized iron powder (RD grade) was used as the base material for the preparation of gas-phase surface-modified soft magnetic composite powders. According to the supplier's technical specification and subsequent elemental verification, the powder possessed high iron purity with limited oxygen content attributed to native surface oxidation formed during production and storage.

The morphology of the as-received powder consisted of irregularly shaped particles with developed surface roughness, typical of atomized iron powders. Representative microstructure of the initial powder is shown in **Figure 4a**, demonstrating pronounced surface asperities and localized porosity.

To ensure suitability for low-frequency soft magnetic composite applications and to reduce interparticle eddy current pathways, the powder was mechanically classified using size separation. Only fractions with particle sizes exceeding 200 μm were selected for further processing. The use of coarse particles is advantageous in reducing the relative volume fraction of insulating material while maintaining high magnetic induction during subsequent compaction.

The chemical composition of the initial iron powder determined by EDS analysis is summarized in **Table 1**.

Table 1. Chemical composition of initial iron powder determined by EDS analysis.

Element	Weight (%)	Atomic (%)
Fe	96.85	89.81
O	3.15	10.19
Total	100.00	100.00

The results confirm that iron is the dominant constituent of the powder, while the detected oxygen originates from thin native oxide films typically present on commercial iron powders. No additional metallic impurities were detected within the sensitivity limits of the analytical technique, indicating high starting material purity suitable for controlled surface modification.

Prior to gas-phase treatment, the powder was subjected to surface passivation in order to suppress uncontrolled oxidation during thermal processing. A high-temperature-resistant silicone-based additive (0.25 wt.% relative to powder mass) was introduced and mechanically distributed using a laboratory-scale ball mill under ambient conditions. The homogenization process ensured uniform additive coverage without inducing plastic deformation or particle fragmentation.

The ball milling setup used for homogenization is presented in **Figure 1**.

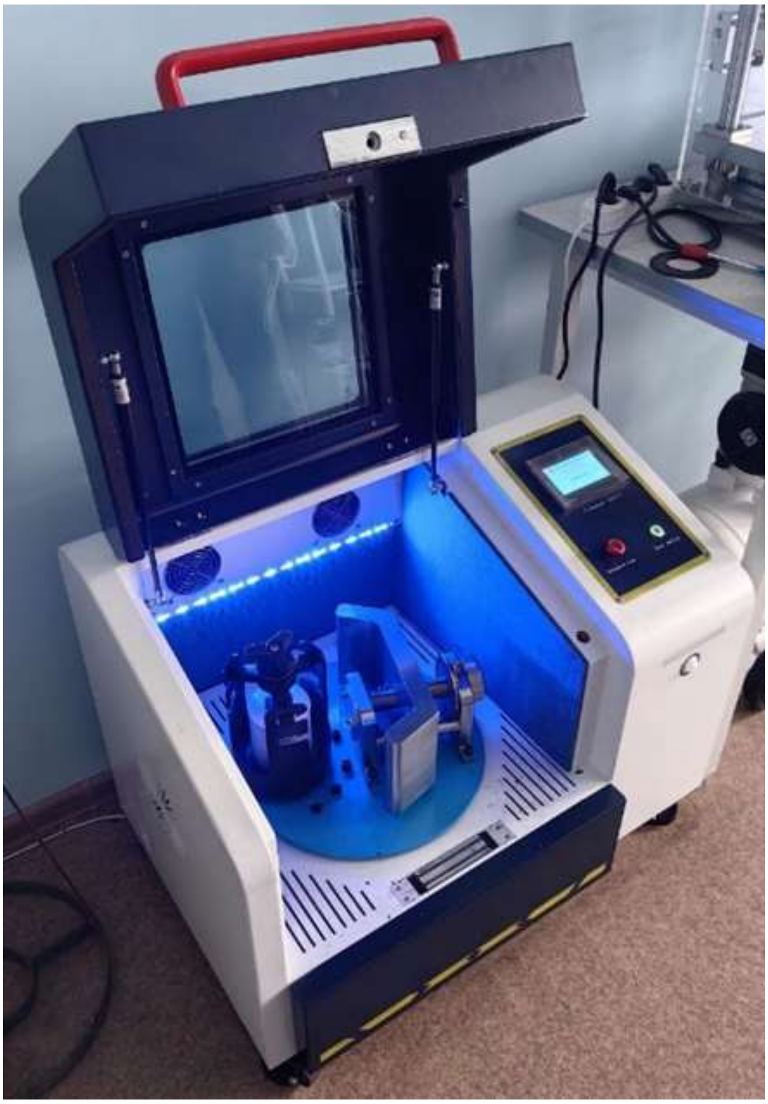

Figure 1. Ball mill used for homogeneous mixing of micron-sized iron powders with passivating and lubricating additives prior to gas-phase coating.

The controlled preparation of the starting powder, including particle size classification and surface passivation, represents a critical preliminary step for achieving reproducible coating formation during subsequent gas-phase phosphating.

2.2. Gas-Phase Insulating Coating Procedure

The electrically insulating surface layer was deposited using a controlled gas-phase phosphating process specifically adapted for micron-sized iron powders. The passivated powder fraction (>200 µm) was placed inside a cylindrical stainless-steel reactor equipped with a rotating drum mechanism to ensure continuous particle agitation during treatment. This dynamic configuration enabled homogeneous exposure of the entire particle surface to the reactive gas atmosphere and minimized local deposition gradients.

The experimental reactor setup is shown in **Figure 2**.

Figure 2. Reactor setup for gas-phase deposition of phosphate-based insulating coatings on iron powder particles under controlled temperature and reduced pressure conditions.

Prior to heating, the reactor chamber was evacuated using a rotary vacuum pump to achieve a residual pressure in the range of 10^{-2}–10^{-3} mmHg. The reduced-pressure environment served two essential purposes: (i) removal of atmospheric oxygen and moisture to suppress uncontrolled oxidation, and (ii) facilitation of uniform vapor-phase transport of the insulating precursor.

After achieving the target vacuum level, the reactor was heated to 200 °C at a controlled heating rate to avoid thermal shock and localized overheating. The selected temperature represents an optimized balance between activation of surface reactions and preservation of the crystalline α-Fe phase. The temperature was maintained throughout the coating cycle to promote controlled surface conversion.

The reactive atmosphere consisted of vapors of a phosphate-forming precursor introduced in combination with a volatile carrier component. Under reduced pressure and elevated temperature, the precursor decomposed and reacted at the iron surface, forming a phosphate-based insulating layer. Continuous mechanical agitation of the powder ensured that particles remained in a quasi-fluidized dynamic state, enabling conformal coating development over complex surface geometries.

To regulate coating thickness, the deposition cycle could be repeated multiple times. Each cycle consisted of:

1. Vacuum stabilization
2. Controlled heating to 200 °C
3. Exposure to reactive vapor phase
4. Gradual removal of volatile components
5. Controlled cooling under reduced pressure

This stepwise deposition strategy enabled precise thickness control ranging from thin nanometric films to thicker micrometric insulating layers without inducing sintering or particle fusion.

After completion of the coating cycle, the reactor was cooled to room temperature under vacuum conditions to minimize post-process oxidation. The treated powders were then removed and stored in sealed containers prior to characterization.

The use of a vacuum-assisted gas-phase route provides several advantages compared to conventional wet phosphating, including improved coating uniformity, reduced solvent contamination, enhanced thickness controllability, and compatibility with scalable powder metallurgy workflows.

2.3. Lubrication and Post-Treatment of Coated Powders

Following gas-phase phosphating, the coated iron powders were subjected to a controlled lubrication and thermal stabilization procedure to improve powder flowability, interparticle rearrangement during compaction, and coating integrity.

A peat-wax-based lubricant was introduced in an amount of 0.15 wt.% relative to the initial powder mass. The lubricant was dissolved in a volatile carrier medium and uniformly distributed over the coated particles using low-energy mechanical mixing in a laboratory-scale ball mill. The mixing was performed under mild conditions to prevent mechanical damage to the phosphate-based insulating layer and to avoid particle fragmentation or coating delamination.

The purpose of lubrication was twofold:

1. To reduce interparticle friction during subsequent compaction;
2. To improve powder flow characteristics and ensure homogeneous die filling.

After lubrication, the composite powder underwent thermal post-treatment inside the same cylindrical reactor used for gas-phase coating. The chamber was evacuated to a pressure of 10^{-2}–10^{-3} mmHg to remove residual atmospheric gases and volatile components introduced during lubrication.

The reactor was then heated to 200 °C and maintained at this temperature for 20 minutes under reduced pressure. This stabilization step served to:

- remove residual solvent traces,
- enhance adhesion between the phosphate-based layer and the iron substrate,
- promote structural relaxation of the coating,
- reduce the risk of microcracking during subsequent mechanical consolidation.

Cooling was carried out under vacuum conditions to minimize re-oxidation of the iron surface. For samples requiring increased insulation thickness, the gas-phase coating and post-treatment cycles were repeated sequentially. The multi-cycle approach enabled systematic control over coating thickness while maintaining crystallographic stability and particle integrity.

The integration of lubrication and thermal stabilization into the processing route ensures compatibility of the coated powders with conventional powder metallurgy workflows, particularly cold pressing and low-temperature consolidation methods.

2.4. Structural and Microstructural Characterization

2.4.1. X-Ray Diffraction (XRD) Analysis

Phase composition and crystallographic stability of both initial and gas-phase treated powders were analyzed using X-ray diffraction (XRD). Measurements were performed using Cu Kα radiation (λ = 1.5406 Å) over a 2θ range of 20°–90°, with a scanning step of 0.02° and a counting time sufficient to ensure adequate signal-to-noise ratio.

Diffraction patterns of the initial and treated powders are presented in **Figure 3**.

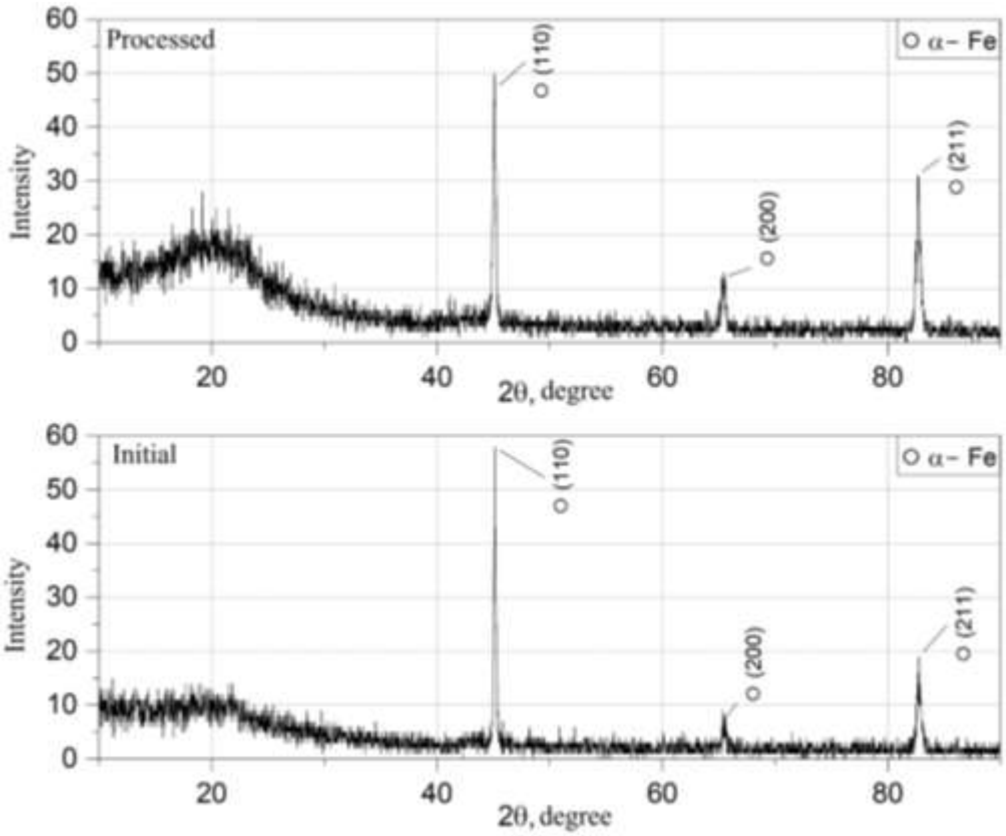

Figure 3. XRD patterns of (a) initial and (b) gas-phase treated iron powders.

The diffraction data were analyzed to identify possible phase transformations, oxide formation, or secondary crystalline compounds induced by thermal exposure during phosphating. Peak positions were compared with standard reference data for body-centered cubic α-Fe. Particular attention was given to potential reflections corresponding to iron oxides or crystalline phosphate phases.

Preservation of the α-Fe phase and absence of additional crystalline peaks were used as criteria for structural stability during gas-phase treatment.

2.4.2. Scanning Electron Microscopy (SEM)

Surface morphology and coating development were investigated using scanning electron microscopy (SEM). Micrographs were acquired at multiple magnifications to evaluate particle shape, surface roughness, and coating continuity.

Representative SEM images of the initial and treated powders are shown in **Figure 4**.

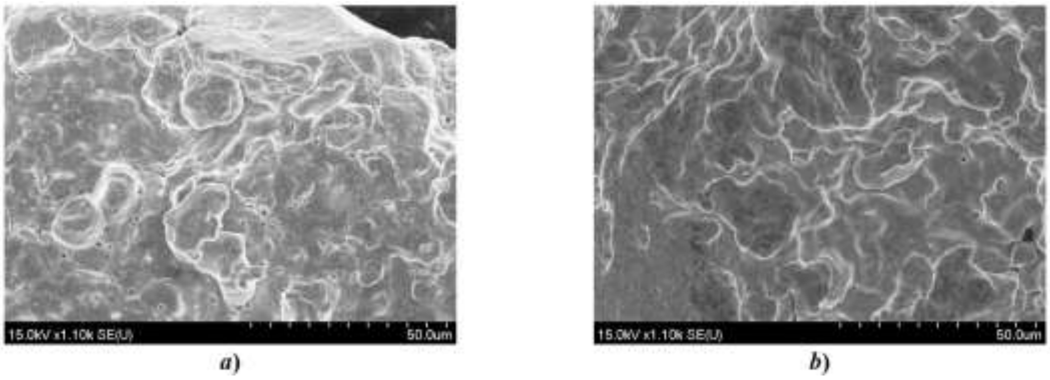

Figure 4. SEM micrographs of iron powder particles: (a) initial powder and (b) gas-phase treated powder. Scale bar: 50 μm.

The initial powder exhibited irregular particle morphology with pronounced surface asperities typical of atomized iron. After gas-phase phosphating, morphological modification was observed, including smoother surface features and indications of conformal surface layer formation.

Qualitative comparison of micrographs was used to assess coating uniformity and detect possible microstructural defects such as cracking, delamination, or localized oxidation.

2.4.3. Energy-Dispersive X-ray Spectroscopy (EDS)

Elemental composition and spatial distribution of chemical elements were determined using energy-dispersive X-ray spectroscopy (EDS) integrated with SEM analysis. Both point analysis and elemental mapping were performed to evaluate phosphorus incorporation and oxygen variation after gas-phase treatment.

The chemical composition of the initial powder is summarized in **Table 1**, while the composition of the treated powder is presented in **Table 2**.

Table 2. Chemical composition of gas-phase treated iron powder determined by EDS analysis.

Element	Weight (%)	Atomic (%)
Fe	90.06	73.88
O	8.25	23.62
P	1.69	2.51
Total	100.00	100.00

Elemental mapping was used to verify coating homogeneity across particle surfaces. Uniform phosphorus distribution without localized enrichment was considered evidence of conformal layer formation. Comparative analysis between initial and treated powders enabled evaluation of chemical modification efficiency.

2.4.4. Data Reliability and Comparative Assessment

All structural and compositional measurements were performed on multiple randomly selected powder regions to ensure statistical representativeness. Comparative evaluation between untreated and treated samples allowed establishment of process–structure correlations.

The integration of XRD, SEM, and EDS provided complementary information regarding crystallographic integrity, surface morphology evolution, and elemental redistribution, forming the basis for the subsequent discussion of coating formation mechanisms.

2.5. Coating Thickness Evaluation and Statistical Analysis

To quantitatively assess the effectiveness of the gas-phase phosphating process, coating thickness and surface coverage were evaluated using cross-sectional SEM observations and image analysis techniques.

Representative cross-sectional micrographs were obtained by embedding treated powder particles in conductive resin followed by mechanical polishing. The thickness of the phosphate-based surface layer was measured at multiple randomly selected locations on at least 20 individual particles to ensure statistical reliability.

The average coating thickness ($\bar{t}$) was calculated as:

$$\bar{t} = \frac{1}{n}\sum_{i=1}^{n} t_i \tag{1}$$

where t_i represents the local coating thickness measured at a given location and n is the total number of measurements.

Standard deviation values were determined to evaluate coating uniformity and reproducibility of the deposition process. A low deviation was considered indicative of homogeneous vapor-phase deposition.

Surface coverage was qualitatively assessed by comparing treated and untreated particle surfaces using high-magnification SEM imaging (see **Figure 4b**). The absence of exposed metallic regions under optimized processing conditions confirmed conformal layer formation.

In addition to thickness evaluation, elemental mapping results were analyzed to verify spatial homogeneity of phosphorus distribution. Regions exhibiting consistent phosphorus intensity across the particle surface were interpreted as uniform coating zones, whereas localized intensity peaks were considered indicators of possible inhomogeneous nucleation.

All measurements were performed in triplicate batches to ensure repeatability of the gas-phase process. The combined structural, morphological, and statistical analyses provide a quantitative basis for correlating processing parameters with coating formation efficiency.

3. Results and Discussion

3.1. Phase Stability During Gas-Phase Phosphating

The XRD patterns of the initial and gas-phase treated powders are shown in Figure 3. The diffraction peaks of the untreated powder correspond to the body-centered cubic (bcc) α-Fe structure, with characteristic reflections observed at approximately 44.7°, 65.0°, and 82.3° (2θ), consistent with standard reference data [1,3].

After gas-phase treatment at 200 °C under reduced pressure, the diffraction patterns reveal no additional crystalline phases within the detection limit of the instrument. The preservation of peak positions and relative intensities confirms that the phosphating process does not induce bulk phase transformation of the iron core under optimized conditions.

The absence of detectable iron oxide peaks suggests that the reduced-pressure environment effectively suppresses uncontrolled oxidation during thermal exposure [12,14]. This result demonstrates that the selected temperature window enables surface conversion reactions without compromising crystallographic stability.

These findings indicate that gas-phase phosphating, when performed under controlled conditions, represents a structurally conservative surface modification route.

3.2. Surface Morphology and Coating Formation

SEM micrographs presented in Figure 4 illustrate significant surface modification after gas-phase treatment. The initial powder (Figure 4a) exhibits irregular morphology with pronounced surface asperities typical of atomized iron particles [10,11].

Following phosphating (Figure 4b), the particle surfaces appear smoother and more uniformly covered. The reduction in sharp asperities and the presence of a continuous surface film indicate the formation of a conformal phosphate-based layer [7–9].

The absence of visible cracks or delamination suggests strong adhesion between the coating and metallic substrate. Additionally, no evidence of particle sintering or neck formation was observed, confirming that the applied thermal conditions remain below the threshold for diffusion-driven consolidation.

The observed morphological evolution supports the hypothesis that gas-phase phosphating proceeds via surface-limited reaction mechanisms rather than bulk diffusion processes.

3.3. Elemental Redistribution and Coating Homogeneity

EDS analysis confirms chemical modification of the particle surfaces after treatment. The initial powder composition (Table 1) is dominated by iron with minor oxygen content originating from native oxide films.

After gas-phase phosphating (Table 2), phosphorus signals are clearly detected, accompanied by a moderate increase in oxygen concentration. This compositional shift is consistent with the formation of a phosphate-based surface layer.

Elemental mapping reveals relatively uniform phosphorus distribution across particle surfaces, with no pronounced localized enrichment zones. The homogeneous elemental coverage suggests that the vacuum-assisted vapor-phase transport mechanism promotes conformal layer development.

The absence of isolated phosphorus-rich clusters indicates controlled nucleation and lateral growth of the coating, rather than discrete particulate deposition.

3.4. Mechanistic Interpretation of Surface Layer Formation

The combined structural and compositional results allow formulation of a mechanistic model for gas-phase phosphating of iron powders [14–16].

Under reduced pressure and elevated temperature, the phosphate precursor decomposes to generate reactive species capable of interacting with the iron surface. Initial adsorption occurs preferentially at high-energy surface sites such as asperities and defect regions. Subsequent lateral growth leads to the formation of a continuous conversion layer [7].

The process can be described as:

1. Surface activation under thermal conditions
2. Adsorption of reactive phosphate species
3. Surface-limited chemical conversion
4. Lateral film growth and coalescence

The absence of bulk phase transformation indicates that the reaction remains confined to the near-surface region. This surface-controlled mechanism explains the preservation of the α-Fe crystalline structure while achieving effective chemical modification.

3.5. Process–Structure Correlations

The results demonstrate that coating formation and structural stability are strongly governed by processing parameters. The selected temperature of 200 °C represents an optimized compromise between reaction activation and oxidation suppression.

At insufficient temperature, incomplete phosphate conversion may occur, leading to non-uniform coverage. Conversely, excessive thermal exposure could promote oxide formation or coating degradation.

Therefore, the gas-phase phosphating process exhibits a defined operational window within which:

- The α-Fe phase remains stable,
- Conformal phosphate layers form,
- Oxidation is minimized,
- Microstructural integrity is preserved.

These correlations provide practical guidance for scaling the process in powder metallurgy and surface engineering applications.

5. Conclusions

A controlled gas-phase phosphating approach was successfully applied to micron-sized iron powders, enabling the formation of conformal phosphate-based surface layers while preserving the crystallographic integrity of the metallic core. X-ray diffraction analysis confirmed retention of the body-centered cubic α-Fe phase under optimized treatment conditions, demonstrating that the selected thermal window prevents bulk phase transformation and excessive oxidation.

Scanning electron microscopy revealed significant surface morphology modification after treatment, characterized by smoother particle surfaces and continuous coating development without evidence of sintering or delamination. Energy-dispersive spectroscopy confirmed phosphorus incorporation and homogeneous elemental distribution, indicating uniform vapor-phase deposition across particle surfaces.

The results establish clear process–structure correlations governing coating formation. The gas-phase phosphating process operates within a defined temperature and pressure window that enables surface-limited chemical conversion while maintaining microstructural stability. Excessive thermal severity may promote localized oxidation and microstructural heterogeneity, highlighting the importance of parameter optimization.

Overall, this study demonstrates that vacuum-assisted gas-phase phosphating represents an effective and controllable route for surface engineering of iron powders. The proposed approach offers improved coating uniformity, reduced oxidation risk, and compatibility with conventional powder metallurgy workflows, providing practical guidance for scalable surface modification of metallic powder systems.

References

1. Meng, B.; Hou, J.; et al. Low-loss and high-induction Fe-based soft magnetic composites coated with magnetic insulating layers. *J. Magn. Magn. Mater.* 2019, *492*, 165651. https://doi.org/10.1016/j.jmmm.2019.165651
2. Grande, M.A.; Ferraris, L.; Francici, F.; Poskovic, E. New SMC material for small electric machines. *IEEE Trans. Ind. Appl.* 2018, *54*, 195–203. https://doi.org/10.1109/TIA.2017.2749426
3. Govor, G.A.; Mihnevich, V.V. Composite soft magnetic materials based on iron powders. *Inorg. Mater.* 2007, *43*, 805–807. https://doi.org/10.1134/S0020168507070129
4. Wu, S.; Li, Y.; Zhang, H.; et al. Processing–structure–property relationships in Fe-based soft magnetic composites prepared by powder metallurgy. *Adv. Powder Mater.* 2023, *2*, 100104. https://doi.org/10.1016/j.apmate.2023.100104
5. Chen, G.; Zhao, H.; Liu, P.; et al. Powder metallurgy routes for low-frequency soft magnetic materials: A review. *Adv. Powder Mater.* 2022, *1*, 100020. https://doi.org/10.1016/j.apmate.2022.100020
6. Rizzi, P.; Ferraris, L.; Poskovic, E. Soft magnetic composites for electrical machines: materials design and industrial perspectives. *IEEE Trans. Magn.* 2020, *56*, 1–9. https://doi.org/10.1109/TMAG.2020.2992014
7. Huang, M.; Zhou, D.; Li, J.; et al. Gas-phase surface modification of metal powders for functional composite materials. *Mater. Des.* 2022, *220*, 110880. https://doi.org/10.1016/j.matdes.2022.110880
8. Matthews, A.; Leyland, A. Developments in vapor phase surface engineering. *Surf. Coat. Technol.* 2002, *149*, 1–8.
9. Sankara Narayanan, T.S.N. Phosphating of steels. *Surf. Coat. Technol.* 1998, *97*, 253–272.
10. Narayanan, T.S.N.S. Surface pretreatment by phosphate conversion coatings—A review. *Rev. Adv. Mater. Sci.* 2005, *9*, 130–177.
11. Liu, X.; Chen, Z.; Wang, Y.; et al. Interface engineering of soft magnetic composites for reduced core losses at low frequencies. *Powder Technol.* 2022, *402*, 117334. https://doi.org/10.1016/j.powtec.2022.117334
12. Kim, J.H.; Park, S.Y.; Lee, K.S.; et al. Scalable fabrication of soft magnetic composites with controlled interparticle insulation. *Acta Mater.* 2022, *230*, 117853. https://doi.org/10.1016/j.actamat.2022.117853
13. Zhang, Y.; Sun, Q.; He, J.; et al. Effect of insulating coating thickness on magnetic losses of Fe-based soft magnetic composites. *J. Magn. Magn. Mater.* 2021, *527*, 167741. https://doi.org/10.1016/j.jmmm.2021.167741
14. Ohring, M. *Materials Science of Thin Films*; Academic Press: San Diego, CA, USA, 2002.
15. Lu, Y.; et al. Vapor-phase deposition mechanisms in surface-modified metal powders. *Mater. Chem. Phys.* 2020, *242*, 122517.
16. Pawlak, Z.; et al. Surface modification of metal powders for advanced applications. *Surf. Eng.* 2015, *31*, 123–130.

17. Totten, G.E. *Steel Heat Treatment: Metallurgy and Technologies*; CRC Press: Boca Raton, FL, USA, 2006.
18. Govor, G.A.; Larin, A.O. Magnetic properties of magnetically soft composite materials. *Inorg. Mater. Appl. Res.* 2019, *10*, 387–390.